Direct Observation of Energy–Momentum Densities in Solids*

E. Weigold, Y. Q. Cai,[A] S. A. Canney,[B] A. S. Kheifets,[B] I. E. McCarthy,[B] P. Storer[C] and M. Vos[B]

Research School of Physical Sciences and Engineering,
Australian National University, Canberra, ACT 0200, Australia.
[A] UVSOR, Institute for Molecular Science, Myodaiji, Okazaki 444, Japan.
[B] Electronic Structure of Materials Centre, Flinders University of
South Australia, GPO Box 2100, Adelaide, SA 5001, Australia.
[C] MCI Ltd, 40 Maple Avenue, Forestville, SA 5035, Australia.

Abstract

Electron momentum spectroscopy (EMS), based on kinematically complete observations of high energy electron impact ionisation events, directly observes energy–momentum dispersion laws and densities of electrons in solids. The valence electronic structure in the near surface region, up to a depth of about 20 Å, is probed for thin free-standing films (about 100 Å) by the multiparameter EMS spectrometer at Flinders University. The principles of the measurement are described and its application to the determination of energy–momentum densities in a range of amorphous, polycrystalline and crystalline materials is discussed.

1. Introduction

Electron momentum spectroscopy (EMS) is the elucidation of the electronic structure of materials by the direct observation of the energy–momentum densities of the electrons determining the chemical and physical properties of the materials. The technique has proved extremely valuable in the understanding of the electronic structure of systems in the gaseous phase, i.e. atoms and molecules (McCarthy and Weigold 1988, 1991). It has now been successfully extended to solids and surfaces, which are much more difficult, but in some respects much more interesting.
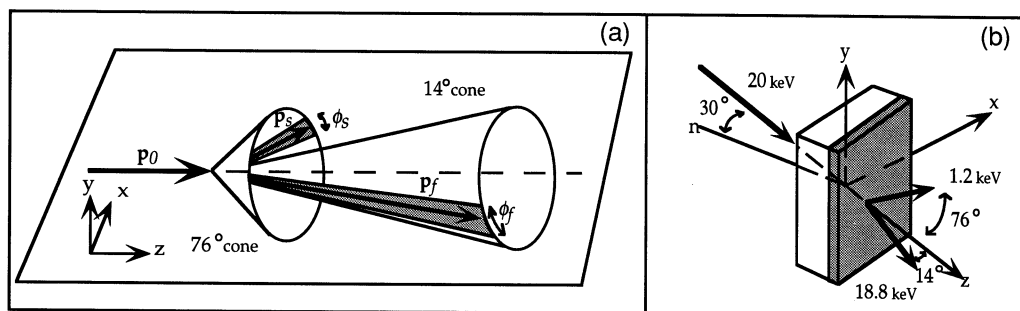
Early EMS studies of solid targets had very poor energy and momentum resolution and very low count rates. Ritter *et al.* (1984) were the first to resolve structure in the valence states of a solid (evaporated carbon films), although they were not able to reveal much detail, since their energy resolution was still only about 6 eV. The coincidence count rates were of the order 0·02 Hz with a momentum resolution of around 0·3 a.u. Williams and Hayes (1990) reported some (e, 2e) measurements on aluminium/aluminium oxide with improved energy resolution (1·5 eV) but with a momentum resolution of 0·45 a.u. and similar low count rates. By comparison the present multi-parameter EMS spectrometer at the ESM Centre, Flinders University (Storer *et al.* 1994) has an energy resolution of better than 1 eV, a momentum resolution of about 0·1 a.u. and for similar target

---

samples has a coincidence count rate of about 4 Hz. The improvement in the data taking rate by more than two orders of magnitude as well as the significant improvement in the energy and the momentum resolutions have ensured that EMS is now a powerful tool in the elucidation of the electronic structure of solids and surfaces.

2. Measurement of Energy–Momentum Densities

The measurement of the energy–momentum densities utilises kinematically complete high-energy electron impact ionisation collisions. Electrons of well-defined energy E_0 and momentum $\mathbf{p}_0$ are directed onto a target consisting of the material to be studied, and the energies and momenta of the two outgoing (scattered and ejected) electrons are determined. In general, one detector, denoted f (for fast), detects electrons that are faster than those in the other detector, denoted s (for slow). The energies and momenta of the detected electrons are denoted by E_f, E_s and $\mathbf{p}_f$, $\mathbf{p}_s$ respectively. The kinematics used in the Flinders spectrometer is shown in Fig. 1.

Fig. 1. The kinematics of the EMS measurements. The momenta of the incident, fast and slow final-state electrons in the (e, 2e) ionisation process are $\mathbf{p}_0, \mathbf{p}_f, \mathbf{p}_s$ respectively. The scattering plane is defined by $\mathbf{p}_0$ and $\mathbf{p}_f$ and the mean scattering plane is the laboratory x–z plane. The polar angles made by $\mathbf{p}_f$ and $\mathbf{p}_s$ with respect to the incident (z) direction are $\theta_f = 14°$ and $\theta_s = 76°$, so that $p_x \sim p_z \sim 0$. The recoil momentum $\mathbf{p}$ (equation 2) is scanned essentially in the y direction by observing events over a range of ϕ_f and ϕ_s. The surface sensitivity is largely determined by the escape depth of the $1 \cdot 2$ keV electron.

The plane formed by $\mathbf{p}_0$ and $\mathbf{p}_f$ is defined to be the scattering plane, the mean scattering plane being horizontal and defines the laboratory x–z plane and the coordinate system (Fig. 1). The coincidence spectrometer (Storer *et al.* 1994) can detect and record events simultaneously in which electrons have suffered a vertical deflection within a predetermined range ($-18° \leq \phi_f \leq 18°$, $\pi - 7° \leq \phi_s \leq \pi + 7°$). The polar angles θ_f and θ_s are chosen so that coplanar events correspond to a billiard-ball collision; that is, to a collision of an electron of momentum $\mathbf{p}_0$ with a stationary free target electron, so that (in the non-relativistic case) the vectors $\mathbf{p}_0$, $\mathbf{p}_f$ and $\mathbf{p}_s$ form a closed right-angled triangle. In the Flinders solid-state spectrometer the energies are chosen to be approximately $E_0 = 20$ keV, $E_s = 1 \cdot 2$ keV and $E_f = 18 \cdot 8$ keV, and the polar angles are $\theta_s = 76°$ and $\theta_f = 14°$. For each coincident pair of detected electrons the electron separation energy or binding energy ε and the recoil momentum $\mathbf{p}$ are recorded:

$$\varepsilon = E_0 - E_f - E_s \,, \tag{1}$$

$$\mathbf{p} = \mathbf{p}_0 - \mathbf{p}_f - \mathbf{p}_s \,. \tag{2}$$

In our experimental configuration the recoil momentum is essentially in the vertical or $\pm y$ direction with $p_x \sim p_z \sim 0$. The spectrometer has been designed to allow θ_s to be changed, which allows momentum components p_y to be measured for non-zero p_z. The use of two-dimensional position-sensitive detectors mounted on the exit planes of the hemispherical (fast electron) and toroidal (slow electron) electrostatic analysers allows the spectrometer to measure simultaneously over a predetermined range of energies E_f and E_s, as well as azimuthal angles ϕ_f and ϕ_s (see Storer *et al.* 1994 for details).

The measurements are done in the transmission mode, i.e. the incident beam passes through a thin sample-target film. The slow $(1 \cdot 2 \text{ keV})$ outgoing electron has by far the lowest mean free path and therefore determines the depth (on the exit side of the film) over which information on the target sample is obtained, typically about 20 Å (see Fig. 1). The surface sensitivity can be increased by tilting the sample to reduce the angle between the slow electron and the surface of the sample.

At high enough energies and high enough momentum transfers $(K = |\mathbf{p}_0 - \mathbf{p}_f|)$ the target electron suffers a clean knock-out, so that the recoil momentum $\mathbf{p}$ is equal and opposite to the momentum $\mathbf{q}$ of the target electron at the collision instant. With this assumption (e, 2e) collisions allow us to directly observe the properties of the target electrons, namely their energies ε and momenta $\mathbf{q}$. The assumption is experimentally verifiable, since the properties attributed to the target electrons must be independent of the way they are observed, in particular, of the incident energy E_0.

For the direct knock-out of an electron we require the concurrence of two events: finding an electron of momentum $\mathbf{q}$ and energy ε [given by its amplitude $\phi_\varepsilon(\mathbf{q})$], and knocking it out with the observed kinematics [given by the antisymmetrised e–e collision cross section $f_{ee}(\mathbf{p}_0, \mathbf{p}_f, \mathbf{p}_s)$]. The unnormalised collision probability that is observed in an (e, 2e) experiment is therefore given by

$$|T|^2 = f_{ee}(\mathbf{p}_0, \mathbf{p}_f, \mathbf{p}_s)|\phi_{\varepsilon i}(\mathbf{q})|^2 \,, \tag{3}$$

where i denotes the symmetry character of the electron ejected (the band for solids or orbital for molecules and atoms from which the electron has been ejected). Under normal EMS conditions (McCarthy and Weigold 1991) f_{ee} is essentially constant, and the unnormalised coincidence count rate $R_{\varepsilon i}(\mathbf{q})$ recorded in the experiment for observed momenta $\mathbf{q}$ and energy ε is

$$R_{\varepsilon i}(\mathbf{q}) = \text{const}|\phi_{\varepsilon i}(\mathbf{q})|^2 = \text{const } \rho_i(\mathbf{q}, \varepsilon) \,, \tag{4}$$

where $\rho_i(\mathbf{q}, \varepsilon)$ is the energy–momentum density of characteristic electrons i.

3. Qualitative Description of the One-electron Energy–Momentum Amplitude

The one-electron energy–momentum amplitude will in general depend on the details of the many-electron wavefunction of the target material. In atoms or

molecules it can be understood as the one-electron overlap between the initial target wavefunction and the wavefunction of the final ion state. In the Green function approach to the many-body problem it corresponds to the amplitude of the one-hole propagator. Electron–electron correlations can influence the amplitude in several ways (McCarthy and Weigold 1988, 1991). Firstly, it can change the density distribution. In molecules such as water, long range correlations in coordinate space lead to considerable enhancement of the density at low values of momenta. Secondly, it can lead to transitions which are forbidden in the independent particle model.

For a solid the amplitude can most simply be understood in terms of the independent particle description of electrons in a crystal. In this model the probability amplitude for finding an electron at the band point $\varepsilon_i(\mathbf{k})$ and at the point $\mathbf{r}$ in coordinate space is the band one-electron function $\Psi_{i\mathbf{k}}(\mathbf{r})$. If we denote the amplitude for an electron in the unit cell, whose centre is the point $\mathbf{R}_n$ of the crystal lattice, by $\psi_i(\mathbf{r} - \mathbf{R}_n)$ then the normalised wavefunction for the band labelled by the unit cell state i is

$$\Psi_{i\mathbf{k}}(\mathbf{r}) = N^{-1/2} \sum_{n=1}^{N} \psi_i(\mathbf{r} - \mathbf{R}_n)e^{i\mathbf{k}\cdot\mathbf{R}_n} , \tag{5}$$

where the number of identical unit cells is N.

The amplitude for finding the electron at point $\mathbf{q}$ in momentum space is then given by the momentum space band wavefunction

$$\Phi_{i\mathbf{k}}(\mathbf{q}) = N^{-1/2}(2\pi)^{-3/2} \int d^3r \ e^{-i\mathbf{q}\cdot\mathbf{r}} \times \sum_{n=1}^{N} \psi_i(\mathbf{r} - \mathbf{R}_n)e^{i\mathbf{k}\cdot\mathbf{R}_n}$$

$$= N^{\frac{1}{2}} \phi_i(\mathbf{k})\delta_{\mathbf{k}-\mathbf{q}} , \tag{6}$$

where the momentum-space orbital of the unit cell is

$$\phi_i(\mathbf{k}) = (2\pi)^{-3/2} \int d^3r \ e^{-i\mathbf{k}\cdot\mathbf{r}}\psi_i(\mathbf{r}) , \tag{7}$$

and the factor

$$\delta_{\mathbf{k}-\mathbf{q}} = N^{-1} \sum_{n=1}^{N} e^{i(\mathbf{k}-\mathbf{q})\cdot\mathbf{R}_n} \tag{8}$$

(for $N \to \infty$) equates the crystal momentum $\mathbf{k}$ to the real observed momentum $\mathbf{q}$.

Valence electrons in a crystal can move from one unit cell to another, so that the boundary conditions of the unit cell orbital are different from those for a molecular orbital, where the wavefunction must decay exponentially. This gives rise to dispersion in energy for electrons in a crystal, whereas for a molecule the electron's energy is independent of $\mathbf{q}$. If the electron were completely free its energy would be simply given by $q^2/2$ (in a.u.).

The separation energy associated with the clean knock-out of an electron is the band energy

$$\varepsilon_i = \varepsilon_i(\mathbf{q}) \,. \tag{9}$$

Events can, however, be observed at other energies due to inelastic scattering processes in the incident or exit channels. Crystal excitation would lead to energy being absorbed in the excitation. In present EMS measurements phonons are not resolved. However, knock-out with the excitation of plasmons (of energy ε_p) by the emitted or incident electrons is observed with the detection of events with energy

$$\varepsilon_{ip} = \varepsilon_i(\mathbf{q}) + \varepsilon_p \,. \tag{10}$$

Inelastic scattering experiments on the target sample at the incident and exit energies allows one to measure the plasmon peaks from the excitation of one or more plasmons, as well as the elastically scattered electrons. These inelastic scattering measurements can then be used to deconvolute the plasmon contributions to the energy–momentum density measurements as discussed by Jones and Ritter (1986).

The assumption that $\mathbf{q} = -\mathbf{p}$ means that the incident and outgoing electrons can be treated as plane waves. In a solid, two elastic 'multiple scattering' processes can occur. The first is diffuse scattering, that is, scattering from atomic cores. The momentum that is transferred to the atomic core can initiate a phonon excitation or is absorbed elastically by the whole lattice. Such events cannot be distinguished energetically from clean knock-out events. The result is a continuous range of momentum transfer $\mathbf{q}_d$ which must be added to $\mathbf{q}$ to obtain the observed recoil momentum

$$\mathbf{p} = \mathbf{q} + \mathbf{q}_d \,. \tag{11}$$

The effect is to spread out the measured momentum profile at a given permitted ε. This diffuse background can be minimised by reducing the sample thickness and hence the number of scattering sites.

The electrons can also be elastically scattered (diffracted) by the collective effect of the crystal planes. This can be described by dynamic diffraction theory (Humphreys 1979) and has been applied to EMS by Allen et al. (1990). Bragg scattering of any of the three high-energy electrons in the reaction adds a reciprocal lattice vector $\mathbf{G}$ to $\mathbf{q}$:

$$\mathbf{p} = -\mathbf{q} + \mathbf{G} \,, \tag{12}$$

and causes a fraction of the peak at $\varepsilon_i(\mathbf{q})$ to be moved to $\varepsilon_i(\mathbf{q} + \mathbf{G})$, with the same dispersion as $\varepsilon_i(\mathbf{q})$. Such 'umklapp' events would be identified by their dispersion. They can be eliminated or minimised by employing suitable chosen energies and crystal orientation.

Although the above analysis is for the independent particle model of crystals, the determination of energy–momentum densities in solids by EMS is, of course, not restricted to them, but can equally well be applied to amorphous and

polycrystalline samples and to surfaces. For polycrystalline samples the energy–momentum densities could to a first approximation be described by the spherically averaged crystal densities. Amorphous materials show no long-range order, and hence could be expected to be more molecular in nature. If the short-range order in the amorphous state is similar to the crystalline state, some of the basic features of the crystalline electronic structures could be conserved. Surface states, on the other hand, could be quite localised and therefore essentially molecular, showing little or no dispersion.
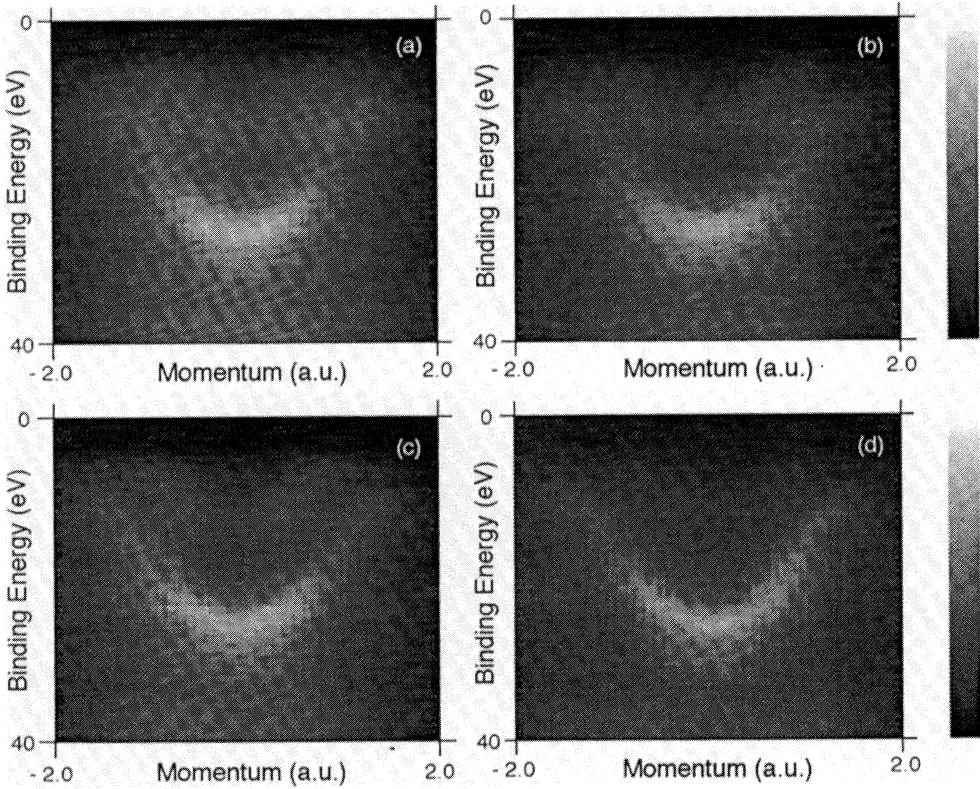
4. Target Preparation and Characterisation

For transmission (e, 2e) experiments it is not possible at present to produce single crystal targets by cleaving under UHV conditions without further processing, such as plasma etching. Using electrochemical and chemical etching it is possible to thin samples to a preliminary stage and then they can be further thinned by plasma etching. The present spectrometer has a target preparation and characterisation facility consisting of two vacuum chambers connected in series with the main collision chamber. The chamber furthest from the collision chamber has a dual function. It serves as a chamber where reactive etch gases can be used and where the etch gas pressure can be maintained in the Torr range. The intermediate buffer chamber (low 10^{-10} Torr range) has an Auger/LEED system for characterising the surface and an annealing stage. Targets can also be prepared in this chamber by evaporation onto one surface of a thin free-standing film. Argon ion sputtering can also take place in this chamber. Target samples can be transferred between the three chambers under vacuum quite rapidly. An attachment to the main chamber allows further characterisation of the sample by means of electron diffraction patterns.

A considerable number of amorphous or polycrystalline targets have been made by evaporating sample material onto a thin amorphous carbon substrate. Samples studied in this way include aluminium, fullerene, silicon, germanium and copper. A 30 Å overlayer of the material is generally sufficient to attenuate the signal from the carbon backing by several orders of magnitude. In some cases such as copper, where 'islands' are formed on evaporation onto the backing, the characteristic carbon energy–momentum density traces underly the sample data. However, since the carbon energy–momentum densities have been accurately measured, they can be subtracted from the data.
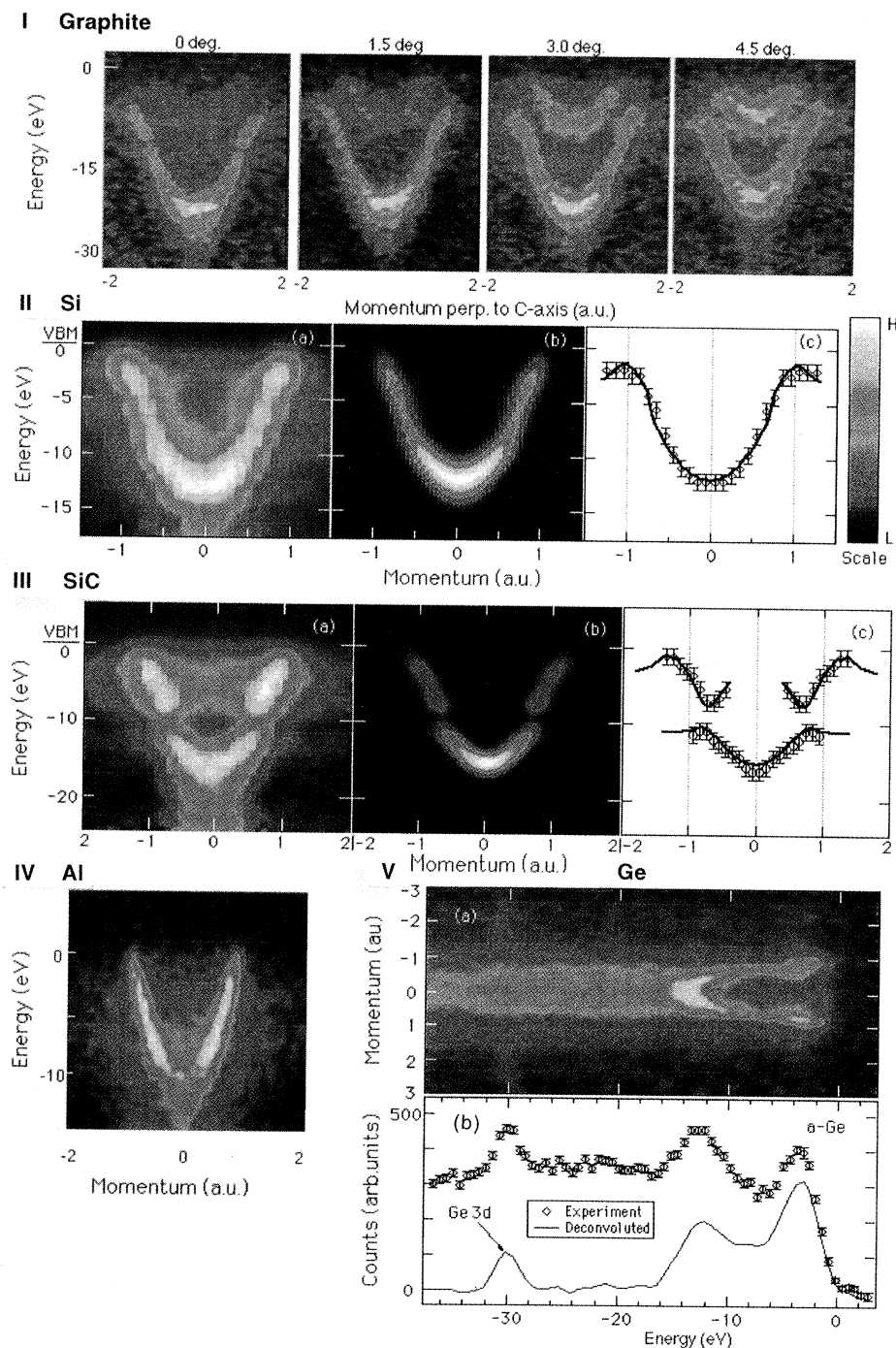
5. Energy–Momentum Densities for Carbon and Some Other Samples

Energy–momentum densities have been obtained for a range of carbon samples. These include amorphous evaporated carbon which is mainly sp^2 bonded, i.e. the short range structure is largely graphitic (Kheifets *et al.* 1994; Vos *et al.* 1995*a*), diamond-like (sp^3) amorphous carbon (Storer *et al.* 1995), crystalline graphite (Vos *et al.* 1994), and fullerene. Fig. 2 shows the valence σ band of an amorphous evaporated carbon sample with increasing annealing, (a)–(c), and of highly oriented pyrolitic graphite (2d). The density is given by a linear grey scale, with the lightest shades showing the regions of highest density. The momentum scale goes from $q_y = -2$ to $+2$ atomic units, with $q_y = 0$ in the centre ($q_x \sim q_z \sim 0$). The separation or binding energy scale is relative to the vacuum.

Fig. 2. Energy–momentum densities for carbon targets plotted on a linear grey scale (zero density being black and higher densities with lighter shading): (a) unannealed evaporated amorphous carbon (e-aC); (b) e-aC annealed by 2 W heating for 10 min; (c) 6 W heating for 10 min; and (d) in-plane momentum density for highly oriented pyrolite graphite.

The momentum density for highly oriented pyrolitic graphite shown in Fig. 2d clearly demonstrates the dispersive σ band, with the highest density at the bottom of the band at $q = 0$. In this sample of graphite there is only relatively short range ordering in the basal planes, but there is a crystal axis, the c axis, ordered uniformly normal to the planes. The momentum density in Fig. 2d is an average over plane orientations for components in the plane. For graphite there is also a π band at higher energies (smaller binding energies) for which symmetry forbids momentum components in the plane through $q_z = 0$ (i.e. the momentum plane with zero component along the c-axis). In the amorphous carbon samples shown in Figs 2a–c the π band is just visible at higher energy and inside the lobes of the σ band. This is particularly so in the highly annealed sample in Fig. 2c. The fact that the amorphous carbon energy–momentum density closely resembles that of graphite shows the graphitic nature of this type of amorphous carbon and the existence of short-range graphite-like order. The short range in the ordering results in a lack of definition of the band. Annealing increases the range of ordering, the target becomes more polycrystalline, and the definition of the band increases. The highly annealed sample in Fig. 2c is very much like polycrystalline graphite, the density resembling spherically averaged graphite crystals, which makes the π band visible. Even after spherical averaging, symmetry requires that the π intensity be zero for zero momentum. The finite momentum resolution leads to some intensity at zero momentum.

I   Graphite

II   Si

III   SiC

IV   Al

V   **Ge**

Fig. 4.   I Measured energy–momentum density for crystalline graphite for different angles $\theta = 76° - \theta_s$ (see Table 1 and text).   II(a) The measured energy–momentum density for amorphous silicon, (b) spherically averaged band calculation for silicon folded with the appropriate resolution functions, and (c) calculated averaged dispersion law (solid curve) compared with experiment.   III As in II except for silicon carbide compared with calculations for cubic SiC.   IV Energy–momentum density for aluminium.   V(a) Energy–momentum density for amorphous germanium and (b) the momentum integrated density showing the deconvolution of measured plasmon excitations from the raw data.

in the valence σ band, and the weaker interplane bonds normal to the surface

band away from $q = 0$. There is no sign of carbon in the data, verifying that the experiment selects the material near the exit side of the sample.

The above silicon–carbon target was then annealed for 10 minutes at temperatures estimated to be at least 600°C in order to see if the definition of the silicon band could be improved. Instead, the resulting energy–momentum density measured by Cai *et al.* (1995) was that shown in Fig. 4III(a). This structure is characteristic of polycrystalline silicon carbide, as can be seen from Fig. 4III(b) which shows the spherically averaged LMTO energy–momentum densities for β-SiC. The antisymmetric gap due to the unequal potentials between the Si and C sites in SiC is clearly visible. The calculated dispersion for the zinc-blende structure of β-SiC is in excellent agreement with the data (Fig. 4III(c)), but as for silicon (Fig. 4II) the calculated density is much lower than the measured one for the high energy regions away from $q = 0$ and in particular beyond the minimum (gap) at the average Brillouin zone edge.

Energy–momentum densities for aluminium, which is a free electron metal, and germanium, a semiconductor, are shown in Figs 4IV and V. Both materials were evaporated under UHV conditions onto carbon films as discussed for silicon above. The dispersion in the case of aluminium is well described by the parabola for a free electron,

$$\varepsilon(q) = W_0 - q^2/2m^*\,,\tag{13}$$

where $m^* = m = 1$ (in a.u.). In the case of germanium a non-dispersive 3d band at $\varepsilon \sim 30$ eV is shown in addition to the dispersive valence band. The 3d electrons are more localised and atomic in nature so that their energy is independent of momentum. The 3d density extends to higher momenta than that of valence band electrons. The deconvolution of measured plasmon excitation events from the experimental data is illustrated in the line diagram in Fig. 4V(b), in which the measured intensity has been integrated over the momentum.

6. Conclusion

We have discussed the recent results obtained with the multiparameter asymmetric EMS spectrometer at Flinders University. The results show that EMS is unique in providing electron energy–momentum density information for the surface region of crystalline, polycrystalline or amorphous solids. The relative importance of the bulk or of the surface of the sample material can be changed by changing the angle the slow emitted electron makes with the surface (e.g. Vos *et al.* 1995c). It is clear that knowledge gained by the new field of EMS of solids and their surfaces should be very useful in furthering our understanding of materials and their application. It is also clear that we can expect further improvements in the technique, both experimental and theoretical, as well as in the data analysis.

References

Allen, L. J., McCarthy, I. E., Maslen, V. W., and Roussouw, C. J. (1990). *Aust. J. Phys.* **43**, 453.

Cai, Y. Q., Vos, M., Storer, P., Kheifets, A. S., McCarthy, I. E., and Weigold, E. (1995). *Phys. Rev.* B **51**, 3449.

Humphreys, L. J. (1979). *Rep. Prog. Phys.* **42**, 1825.

Jones, R., and Ritter, A. L. (1986). *J. Elect. Spectrosc. Rel. Phen.* **40**, 285.

Kheifets, A. S., and Cai, Y. Q. (1995). *J. Phys.* C **7**, 1821.

Kheifets, A. S., Lower, J., Nygaard, K. J., Utteridge, S., Vos, M., Weigold, E., and Ritter, A. L. (1994). *Phys. Rev.* B **49**, 2113.

McCarthy, I. E., and Weigold, E. (1988). *Rep. Prog. Phys.* **51**, 299.

McCarthy, I. E., and Weigold, E. (1991). *Rep. Prog. Phys.* **54**, 789.

Ritter, A. L., Dennison, J. R., and Jones, R. (1984). *Phys. Rev. Lett.* **53**, 2054.

Storer, P., Cai, Y. Q., Canney, S. A., Clark, S. A. C., Kheifets, A. S., McCarthy, I. E., Utteridge, S., Vos, M., and Weigold, E. (1995). *J. Phys.* D (in press).

Storer, P. J., Caprari, R. S., Clark, S. A. C., and Weigold, E. (1994). *Rev. Sci. Instrum.* **65**, 2214.

Vos, M., Storer, P., Canney, S. A., Kheifets, A. S., McCarthy, I. E., and Weigold, E. (1994). *Phys. Rev.* B **50**, 5635.

Vos, M., Storer, P., Cai, Y. Q., McCarthy, I. E., and Weigold, E. (1995*a*). *Phys. Rev.* B **51**, 1866.

Vos, M., Storer, P., Cai, Y. Q., Kheifets, A. S., McCarthy, I. E., and Weigold, E. (1995*b*). *J. Phys.* C **7**, 279.

Vos, M., Canney, S. A., Storer, P., McCarthy, I. E., and Weigold, E. (1995*c*). *Surf. Sci.* **327**, 387.

Williams, J. F., and Hayes, P. A. (1990). *Aust. J. Phys.* **43**, 465.